 https://doi.org/10.3311/PPee.37305

Periodica Polytechnica Electrical Engineering and Computer Science, 68(4), pp. 344–355, 2024

A New Modeling Approach and Comprehensive Monitoring of Electrical Faults Through Spectral Analysis in DSIM

Samira Chekkal Ait Ouaret[1*], Yacine Imaouchen[2], Djamal Aouzellag[1], Kaci Ghedamsi[1]

[1] Université de Bejaia, Faculté de Technologie, Laboratoire de Maitrise des Energies Renouvelables, 06000 Bejaia, Algérie
[2] Université de Bejaia, Faculté de Technologie, Laboratoire de Génie Electrique Bejaia, 06000 Bejaia, Algérie
[*] Corresponding author, e-mail: samira.chekkal@univ-bejaia.dz

Received: 09 May 2024, Accepted: 01 July 2024, Published online: 06 August 2024

Abstract

The objective of this study is to evaluate the dependability of double-star induction machines by employing meticulous monitoring and intelligent handling of potential electrical malfunctions that may arise during their functioning. Specifically, the research delves into the examination of three distinct fault types: rotor bar breakage, stator phase opening, and inter-turn short circuit. Utilizing a mathematical model developed in the natural reference frame (abc), our aim is to comprehensively delineate both normal and faulty operational scenarios. To categorize and gauge the gravity of identified faults, we employ a methodology rooted in spectral analysis. In order to ensure continuous machine operation, especially in instances of stator phase opening, our proposed mitigation approach entails intentionally opening a secondary phase positioned at a 90-degree angle to the faulty phase. This strategic alteration transforms the machine into a dual two-phase configuration. Through rigorous simulation analyses, our findings underscore the efficacy and pragmatic viability of the devised fault detection technique, offering valuable insights into the domain of electrical machine reliability and fault management.

Keywords

dual-star induction machine (DSIM), broken bars, open phase, short-circuit, modeling in the abc natural reference frame

1 Introduction

Asynchronous machines pose significant concerns in industrial settings due to frequent production interruptions from mechanical or electrical issues, resulting in substantial costs. This study explores improving machine performance by replacing the traditional three-phase winding with a higher number of phases, enhancing reliability, torque quality, and fault tolerance [1, 2]. The double star asynchronous machine emerges as a robust and efficient solution, ideal for reliable applications [3–5]. With fault tolerance becoming crucial, this design evolution holds promise for enhancing industrial system durability and performance [6]. Degradation of asynchronous motor bars is influenced by factors like direct starting and unexpected mechanical variations, causing thermal and mechanical stresses beyond design limits [7, 8]. Softer starting methods and rigorous quality control are recommended [7]. Diagnostic signals, including stator current, Park vector, and mechanical vibration, offer crucial information for maintenance [9–10]. Various techniques, like Fourier transform analysis, face limitations, but machine learning-based approaches show high recognition rates [11–13]. A novel Hilbert transform method for stator current envelope analysis shows promise [14]. Stator winding faults arise from diverse issues, leading to circuit interruptions, overheating, and machine damage [15]. Stator inter-turn short faults are particularly dangerous, potentially escalating to phase-to-phase and phase-to-ground short circuit [6, 16]. Some research results introduce a technique using Random Forest and Park's Vector methods for fault identification, requiring real-world validation [17]. Researchers [18] propose a VI loci-based technique for stator inter-turn short-circuit detection in low-power motors, urging wider adoption, while also discussing frequency response analysis for stator winding fault detection with potential challenges in practical effectiveness and accuracy [19]. Additionally, a fault diagnosis method is introduced for high-speed solid-rotor induction motors, raising questions about its practical applicability [20]. Moreover, a robust control approach is presented for a wind turbine system with a dual-star induction generator, emphasizing stability and fault detection, albeit potentially overlooking dynamic responses under varying conditions

Cite this article as: Chekkal Ait Ouaret, S., Imaouchen, Y., Aouzellag, D., Ghedamsi, K. "A New Modeling Approach and Comprehensive Monitoring of Electrical Faults Through Spectral Analysis in DSIM", Periodica Polytechnica Electrical Engineering and Computer Science, 68(4), pp. 344–355, 2024.
https://doi.org/10.3311/PPee.37305

and predictive maintenance strategies [21]. Other studies present a sensorless modelling and control approach for five-phase open-wound induction machines, but highlight the challenges associated with the complexity of the models and algorithms, suggesting simplification to enhance reliability in industrial environments [22]. Our study specifically addresses rotor bar breakage, stator phase opening, and short-circuit between turns in a dual-star induction machine with a squirrel-cage rotor, favoring its windings for improved energy efficiency and service continuity. The linear system with a stator featuring two identical windings and a squirrel-cage rotor will be detailed further in the paper, excluding considerations for the saturation effect of magnetic material.

2 Model of asynchronous machine

2.1 The modified squirrel cage

Fig. 1 portrays a simplified cage winding (a) alongside phasors (b), which illustrate both bar and ring currents. The bars are numbered in sequence from 1 to Q_r, and the arrows indicate their respective positive directions. The resistance of only one bar is represented by r_{bar}, while its inductance is denoted by I_{bar}. Additionally, r_{ring} and I_{ring} symbolise the parameters of the section of the ring positioned between two bars. The overall impedance of the winding is calculated accordingly. A phase diagram representing the current is generated for the rotor bars at harmonic v, with a phase shift of $v\alpha_u p$ for the angular position of each bar. Owing to the adaptable nature of squirrel cage rotors to operate with various numbers of stator pole pairs, α_u is adopted as the mechanical angle, synchronised with the electrical angle of $p\alpha_u$ (as illustrated in Fig. 1). Then a polygon is constructed to provide a graphical representation of the bar currents [23].

At every junction between the bar and the ring, Kirchhoff's first law is upheld-as illustrated in Fig. 1 (a).

$$\underline{I}_{\text{ring},x} = \underline{I}_{\text{bar},x} + \underline{I}_{\text{ring},x-1} \,. \tag{1}$$

Furthermore, the mutually phase angle between the circular currents is $v\alpha_u p$. The phase difference between the currents of the two ring segments is αp. Each bar comprises a single winding in a rotor phase, with the number of turns represented by $N_r = 1/2$. The current flowing through a bar corresponds to the rotor phase current. Referring to Fig. 1 (b), the RMS value of the induced current in one bar is denoted as I_{bar}.

Consequently, we derive the current in the ring as follows:

$$I_{\text{ring}} = \frac{I_{\text{barv}}}{2 \cdot \sin\left(\dfrac{p\pi}{Qr}\right)} \,. \tag{2}$$

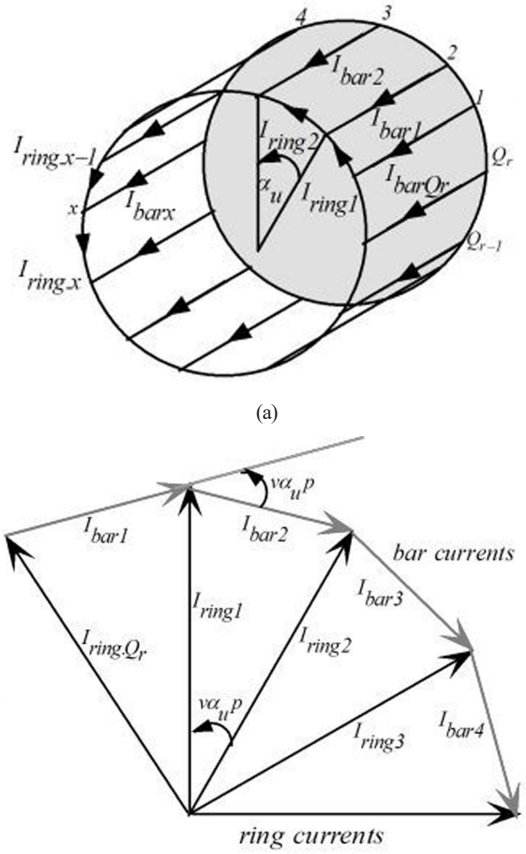

Fig. 1 (a) Diagram for a cage winding and (b) a sector of a polygon of the phasors of the bar currents and a section of the current phasor diagram [23]

The expressions for the rotor resistance and leakage inductance of one rotor bar with the addition of the proportion of short-circuit rings are written as follows:

$$r_r = r_{\text{bar}} + \frac{r_{\text{ring}}}{2 \cdot \sin^2\left(\dfrac{p\pi}{Qr}\right)}, \tag{3}$$

$$l_r = l_{\text{bar}} + \frac{l_{\text{ring}}}{2 \cdot \sin^2\left(\dfrac{p\pi}{Qr}\right)}. \tag{4}$$

Where: r_r and l_r: Resistance and leakage inductance of a one-bar (with the addition of the proportion of short-circuit rings), respectively; r_{ring} and I_{ring}: Resistance and leakage inductance of short-circuit ring, respectively. Fig. 2 illustrates the squirrel cage both before and after incorporating the ring proportions into the rotor bars.

In this section, we present the mathematical model of the machine under study in the natural system of coordinates (ABC), neglecting spatial harmonics.

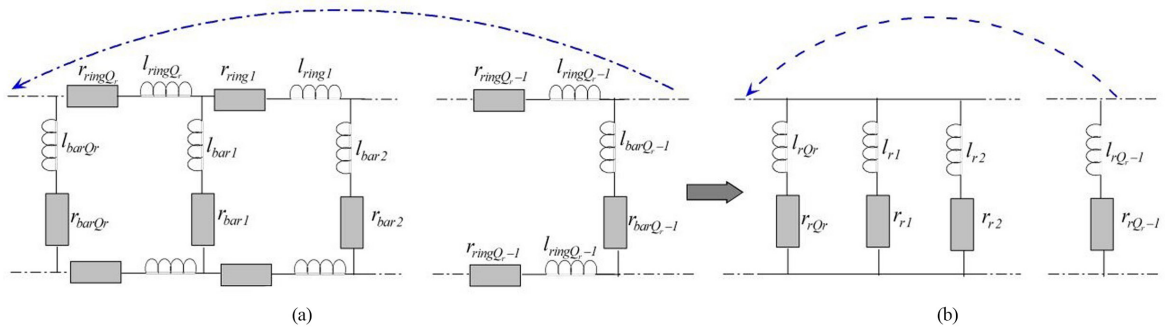

Fig. 2 (a) Squirrel cage before adding the ring proportions to the rotor bars; (b) Squirrel cage after adding the ring proportions to the rotor bars

2.2 Mathematical model of the dual star induction machine

The double-star asynchronous machine under study consists of two stars, each with three stator phases and 38 rotor phases (rotor bars).

2.2.1 Electrical equations

The electrical equations of the machine, expressed in the natural coordinate system (ABC), are as follows:

$$\begin{cases} [\bar{v}_{s1}] = [r_{s1}][i_{s1}] + \dfrac{[d\psi_{s1}]}{dt} \\ [\bar{v}_{s2}] = [r_{s2}][i_{s2}] + \dfrac{[d\psi_{s2}]}{dt} \\ [\bar{v}_{r}] = [r_{r}][i_{r}] + \dfrac{[d\psi_{r}]}{dt} \end{cases}. \tag{5}$$

2.2.2 Magnetic equations

The expressions of the stator and rotor flows are given by the following matrix form:

$$\begin{cases} [\psi_{s1}] = [L_{s1,s1}][i_{s1}] + [M_{s1,s2}][i_{s2}] + [M_{s1,r}][i_{r}] \\ [\psi_{s2}] = [L_{s2,s2}][i_{s2}] + [M_{s2,s1}][i_{s1}] + [M_{s2,r}][i_{r}] \\ [\psi_{r}] = [L_{r,r}][i_{r}] + [M_{r,s1}][i_{s1}] + [M_{r,s2}][i_{s2}] \end{cases}. \tag{6}$$

With:

$$[L_{s1,s1}] = [L_{s2,s2}] = \begin{bmatrix} l_{fs}+l_{ms} & \dfrac{-l_{ms}}{2} & \dfrac{-l_{ms}}{2} \\ \dfrac{-l_{ms}}{2} & l_{fs}+l_{ms} & \dfrac{-l_{ms}}{2} \\ \dfrac{-l_{ms}}{2} & \dfrac{-l_{ms}}{2} & l_{fs}+l_{ms} \end{bmatrix},$$

$$\begin{aligned} &[v_{s1}] = [v_{as1} \quad v_{bs1} \quad v_{cs1}]^t; \\ &[i_{s1}] = [i_{as1} \quad i_{bs1} \quad i_{cs1}]^t; \\ &[\psi_{s1}] = [\psi_{as1} \quad \psi_{bs1} \quad \psi_{cs1}]^t; \\ &[v_r] = [v_{r1} v_{r2} v_{r3} \ldots v_{rj} \ldots v_{rQ_r}]^t = 0_{Qr}; \\ &[i_r] = [i_{r1} i_{r2} i_{r3} \ldots i_{rj} \ldots i_{rQ_r}]^t; \\ &[\psi_r] = [\psi_{r1} \psi_{r2} \psi_{r3} \ldots \psi_{rj} \ldots \psi_{rQ_r}]^t; \\ &[r_{s1}] = diag([r_{as1} r_{bs1} r_{cs1}]); \\ &[r_{s2}] = diag([r_{as2} r_{bs2} r_{cs2}]); \\ &[r_r] = diag([r_{r1} r_{r2} \ldots r_{rj} \ldots r_{rQ_r}]). \end{aligned} \tag{7}$$

$$[L_{r,r}] \begin{bmatrix} L_{rr}+l_{mb} & l_{mb}\cos\left(\frac{2\pi}{Q_r}\right) & l_{mb}\cos\left(\frac{2.2\pi}{Q_r}\right) & l_{mb}\cos\left(\frac{3.2\pi}{Q_r}\right) & \cdots & l_{mb}\cos\left(\frac{(Q_r-1)2\pi}{Q_r}\right) \\ l_{mb}\cos\left(\frac{2\pi}{Q_r}\right) & L_{rr}+l_{mb} & l_{mb}\cos\left(\frac{2\pi}{Q_r}\right) & l_{mb}\cos\left(\frac{2.2\pi}{Q_r}\right) & \cdots & l_{mb}\cos\left(\frac{(Q_r-2)2\pi}{Q_r}\right) \\ l_{mb}\cos\left(\frac{2.2\pi}{Q_r}\right) & l_{mb}\cos\left(\frac{2\pi}{Q_r}\right) & L_{rr}+l_{mb} & l_{mb}\cos\left(\frac{2\pi}{Q_r}\right) & \cdots & l_{mb}\cos\left(\frac{(Q_r-3)2\pi}{Q_r}\right) \\ l_{mb}\cos\left(\frac{3.2\pi}{Q_r}\right) & l_{mb}\cos\left(\frac{2.2\pi}{Q_r}\right) & l_{mb}\cos\left(\frac{2\pi}{Q_r}\right) & \ddots & \cdots & l_{mb}\cos\left(\frac{(Q_r-4)2\pi}{Q_r}\right) \\ \vdots & \vdots & \vdots & \cdots & & \ddots \vdots \\ l_{mb}\cos\left(\frac{(Q_r-1)2\pi}{Q_r}\right) & l_{mb}\cos\left(\frac{(Q_r-2)2\pi}{Q_r}\right) & l_{mb}\cos\left(\frac{(Q_r-3)2\pi}{Q_r}\right) & l_{mb}\cos\left(\frac{(Q_r-4)2\pi}{Q_r}\right) & \cdots & L_{rr}+l_{mb} \end{bmatrix}. \tag{8}$$

Matrices of stator and rotor inductors respectively; l_{fs} and l_{rr}: Stator and rotor leakage inductors, respectively; l_{ms} and l_{mb}: Maximum stator and rotor magnetization inductors, respectively.

With: $m_{sr} = \sqrt{l_{ms} \cdot l_{mb}}$: Maximum mutual inductance between stator phase and corresponding rotor phase; $\left[M_{r,s1}\right] = \left[M_{s1,r}\right]^t$: Coupling inductance matrices between star1 and rotor and vice versa; $\left[M_{r,s2}\right] = \left[M_{s2,r}\right]^t$: Coupling inductance matrices between star2 and rotor and vice versa.

After the development of the two Eqs (5) and (6), we obtain the system of Eq (11).

$$\left[M_{s1,r}\right] = m_{sr}\begin{bmatrix} \cos\left(\theta_r + \frac{\pi}{Q_r}\right) & \cos\left(\theta_r + \frac{3\pi}{Q_r}\right) & \cos\left(\theta_r + \frac{5\pi}{Q_r}\right) & \cdots & \cos\left(\theta_r + \frac{(2Q_r-1)\pi}{Q_r}\right) \\ \cos\left(\theta_r + \frac{\pi}{Q_r} + \frac{2\pi}{3}\right) & \cos\left(\theta_r + \frac{3\pi}{Q_r} + \frac{2\pi}{3}\right) & \cos\left(\theta_r + \frac{5\pi}{Q_r} + \frac{2\pi}{3}\right) & \cdots & \cos\left(\theta_r + \frac{(2Q_r-1)\pi}{Q_r} + \frac{2\pi}{3}\right) \\ \cos\left(\theta_r + \frac{\pi}{Q_r} + \frac{2\pi}{3}\right) & \cos\left(\theta_r + \frac{3\pi}{Q_r} + \frac{2\pi}{3}\right) & \cos\left(\theta_r + \frac{5\pi}{Q_r} + \frac{2\pi}{3}\right) & \cdots & \cos\left(\theta_r + \frac{(2Q_r-1)\pi}{Q_r} + \frac{2\pi}{3}\right) \end{bmatrix}, \tag{9}$$

$$\left[M_{s2,r}\right] = m_{sr}\begin{bmatrix} \cos\left(\theta_r - \alpha + \frac{\pi}{Q_r}\right) & \cos\left(\theta_r - \alpha + \frac{3\pi}{Q_r}\right) & \cos\left(\theta_r - \alpha + \frac{5\pi}{Q_r}\right) & \cdots & \cos\left(\theta_r - \alpha + \frac{(2Q_r-1)\pi}{Q_r}\right) \\ \cos\left(\theta_r - \alpha + \frac{\pi}{Q_r} - \frac{2\pi}{3}\right) & \cos\left(\theta_r - \alpha + \frac{3\pi}{Q_r} - \frac{2\pi}{3}\right) & \cos\left(\theta_r - \alpha + \frac{5\pi}{Q_r} - \frac{2\pi}{3}\right) & \cdots & \cos\left(\theta_r - \alpha + \frac{(2Q_r-1)\pi}{Q_r} - \frac{2\pi}{3}\right) \\ \cos\left(\theta_r - \alpha + \frac{\pi}{Q_r} + \frac{2\pi}{3}\right) & \cos\left(\theta_r - \alpha + \frac{3\pi}{Q_r} + \frac{2\pi}{3}\right) & \cos\left(\theta_r - \alpha + \frac{5\pi}{Q_r} + \frac{2\pi}{3}\right) & \cdots & \cos\left(\theta_r - \alpha + \frac{(2Q_r-1)\pi}{Q_r} + \frac{2\pi}{3}\right) \end{bmatrix}, \tag{10}$$

$$\begin{cases} \frac{d}{dt}\left[i_{s1}\right] = \left[L_{s1,s1}\right]^{-1}\left\{\left[v_{s1}\right] - \left[r_{s1}\right]\left[i_{s1}\right] - \left[M_{s1,r}\right]\frac{d}{dt}\left[i_r\right] - \omega_r\left\{\frac{d}{d_{\theta r}}\left[M_{s1,r}\right]\right\}\left[i_r\right]\right\} \\ \frac{d}{dt}\left[i_{s2}\right] = \left[L_{s2,s2}\right]^{-1}\left\{\left[v_{s2}\right] - \left[r_{s2}\right]\left[i_{s2}\right] - \left[M_{s2,r}\right]\frac{d}{dt}\left[i_r\right] - \omega_r\left\{\frac{d}{d_{\theta r}}\left[M_{s2,r}\right]\right\}\left[i_r\right]\right\} \\ \frac{d}{dt}\left[i_r\right] = \left[L_{r,r}\right]^{-1}\left\{\begin{array}{l}\left[v_r\right] - \left[r_r\right]\left[i_r\right] - \left[M_{s1,r}\right]\frac{d}{dt}\left[i_{s1}\right] - \left[M_{s2,r}\right]\frac{d}{dt}\left[i_{s2}\right] \\ -\omega_r\left\{\frac{d}{d_{\theta r}}\left[M_{s1,r}\right]\right\}\left[i_{s1}\right] - \omega_r\left\{\frac{d}{d_{\theta r}}\left[M_{s2,r}\right]\right\}\left[i_{s2}\right]\end{array}\right\} \end{cases}. \tag{11}$$

2.2.3 Electromagnetic torque equation

The expression of the electromagnetic torque is reduced to:

$$T_{em} = p\left(\left[i_{s1}\right]^t \frac{d}{d\theta_r}\left[M_{s1,r}\right]\left[i_r\right] + \left[i_{s2}\right]^t \frac{d}{d\theta_r}\left[M_{s2,r}\right]\left[i_r\right]\right). \tag{12}$$

Where: p Number of pair poles.

2.2.4 Mechanical equation

The general equation of the speed rotation of the machine is written:

$$J\frac{d\Omega_r}{dt} = T_{em} - T_r - K_f \&_r . \tag{13}$$

With: J Total inertia; K_f: viscous friction; Ω_r: Rotor mechanical speed.

2.3 Opening of stator phase

The electrical equation of the generator can be defined when there is stator phase opening as follows:

$$[r_{s1}] = diag\left(\left[r_{f1} + r_{as1}\ \ r_{bs1}\ \ r_{cs1}\right]\right), \tag{14}$$

$$[r_{s2}] = diag\left(\left[r_{as2}\ \ r_{bs2}\ \ r_{f2} + r_{cs2}\right]\right). \tag{15}$$

With: $r_{f1} = r_{f2} = \begin{cases} 0 & \text{Closed circuit} \\ \text{Very high value} & \text{Open circuit} \end{cases}$.

2.4 Short-circuit between turns in the 1st stator phase of star 1

The appearance of a stator short-circuit indicates the presence of a low-resistance connection or a direct short-circuit between two or more stator windings. This can occur when the electrical insulation between the windings breaks down, allowing excessive current to flow through the short circuit. To gain a better understanding of the possible malfunctioning of the machine, it is essential to develop a detailed mathematical model describing its behaviour in the event of a short-circuit. Then, the use of Matlab software [24] is of crucial importance to solve the non-linear equations and collect the data essential to the analysis. Fig. 3 shows an example of a short- circuit in the winding of the first stator phase 01.

To design the appropriate system to be implemented, we have taken into account certain simplifying hypotheses: The fault occurred at the stator level in the winding of the phase (a_s) of the 1st star, the resistance (r_{f1}) is considered as a fault resistance, we take $r_{f1} = 0$, the phase voltage (a_s) of the 1st star is assumed to be equal to the sum of the two voltages, the coefficient μ represents the number of short-circuited turns relative to the total number of turns of the winding of phase a_s of the 1st star:

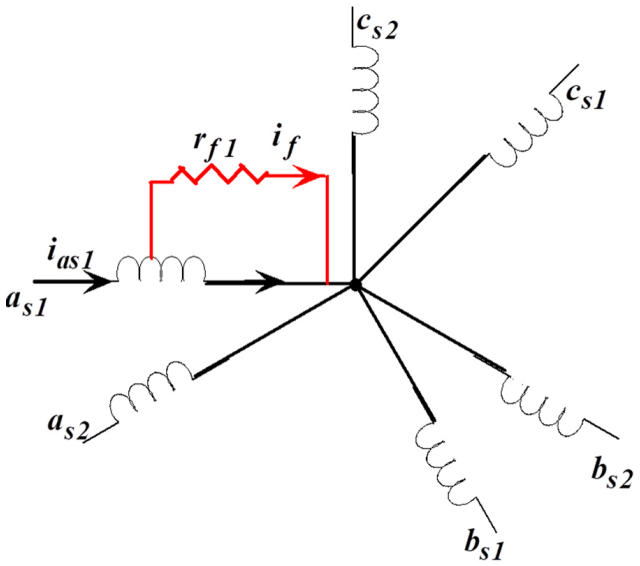

Fig. 3 Diagram illustrating the two stator windings of the studied MASDE with a short circuit occurring in its a_{s1} phase

$$\mu = \frac{N_{asc}}{N_{as1} + N_{asc}} = \frac{N_{asc}}{N_{as}}. \tag{16}$$

Where: N_{as}: Turns per phase number; N_{as1}, N_{asc}: Number of turns of the two parts of the phase in short-circuit.

2.4.1 Electrical equations

The electric equation of the generator can be defined in the case ofinter-turn short faulton phase a_{s1} as:

$$\begin{cases} v_{as1} = r_{as1} i_{as1} + \dfrac{d\varphi_{as1}}{dt} \\ v_{bs1} = r_{bs1} i_{bs1} + \dfrac{d\varphi_{bs1}}{dt} \\ v_{cs1} = r_{cs1} i_{cs1} + \dfrac{d\varphi_{cs1}}{dt} \\ v_{csc} = r_{asc} i_{asc} + \dfrac{d\varphi_{asc}}{dt} \end{cases}. \tag{17}$$

The resistance matrix r_{s1} can be defined as follows:

$$[r_{s1}] = \begin{bmatrix} r_{as1} & 0 & 0 & -r_{f1} \\ 0 & r_{bs1} & 0 & 0 \\ 0 & 0 & r_{cs1} & 0 \\ -r_{f1} & 0 & 0 & r_{sc} \end{bmatrix}. \tag{18}$$

Where: $r_{as1} = (1-\mu) \cdot r_{s1} + r_f$; $r_{sc} = \mu r_{s1} + r_{f1}$.

The stator inductance matrix of the first star with this type of stator fault is written as:

$$[L_{s1,s1}] = l_{s1}\begin{bmatrix} (1-\mu)^2 & 0 & 0 & 0 \\ 0 & 1 & 0 & 0 \\ 0 & 0 & 1 & 0 \\ 0 & 0 & 0 & \mu^2 \end{bmatrix} + l_{ms}\begin{bmatrix} (1-\mu)^2 & \frac{-(1-\mu)}{2} & \frac{-(1-\mu)}{2} & \mu(1-\mu) \\ \frac{-(1-\mu)}{2} & 1 & \frac{-1}{2} & \frac{-\mu}{2} \\ \frac{-(1-\mu)}{2} & \frac{-1}{2} & 1 & \frac{-\mu}{2} \\ \mu(1-\mu) & \frac{-\mu}{2} & \frac{-\mu}{2} & \mu^2 \end{bmatrix}. \tag{19}$$

The matrices of the coupling inductances between the two stator stars and the rotor and vice versa are written as:

$$[L_{s2,s2}] = \begin{bmatrix} l_{s2} + l_{ms} & \frac{-l_{ms}}{2} & \frac{-l_{ms}}{2} \\ \frac{-l_{ms}}{2} & l_{s2} + L_{ms} & \frac{-l_{ms}}{2} \\ \frac{-l_{ms}}{2} & \frac{-l_{ms}}{2} & l_{s2} + l_{ms} \end{bmatrix}. \tag{20}$$

3 Simulation results

3.1 Broken rotor bars in the cage of dual-star induction machine

In order to create a diagnostic procedure, a simulation is carried out in the MATLAB/Simulink environment. The aim of this simulation is to observe how the differential variables behave both under normal operating conditions and in the event of a fault.

We then obtain a state system which governs the behaviour of the electrical part of the double star machine represented by the system of Eq. (25).

In this simulation, we considered several scenarios. Initially, we assumed that the machine was operating normally without any problems. At time t = 1.5 s, we introduced a load torque of 100 N.m (nominal), simulating a disturbance in the system. At time t = 3 s, we modeled the breakage of a rotor bar, which had a significant impact on the machine's behavior. Finally, at time t = 4.5 s, we simulated the breakage of a second rotor bar, which further altered the machine's operating conditions. These parameters and specific events enable us to analyze the machine's behavior in a variety of situations and to understand how it reacts to these disturbances.

$$\left[L_{s1,s2}\right]=l_{ms}\begin{bmatrix}(1-\mu)\cos(\alpha) & (1-\mu)\cos\left(\alpha+\frac{2\pi}{3}\right) & (1-\mu)\cos\left(\alpha+\frac{4\pi}{3}\right)\\ \cos\left(\alpha+\frac{4\pi}{3}\right) & \cos(\alpha) & \cos\left(\alpha+\frac{2\pi}{3}\right)\\ \cos\left(\alpha+\frac{2\pi}{3}\right) & \cos\left(\alpha+\frac{4\pi}{3}\right) & \cos(\alpha)\\ (\mu)\cos(\alpha) & (\mu)\cos\left(\alpha+\frac{2\pi}{3}\right) & (\mu)\cos\left(\alpha+\frac{4\pi}{3}\right)\end{bmatrix}, \tag{21}$$

$$\left[L_{s1,r}\right]=m_{sr}\begin{bmatrix}(1-\mu)\cos\left(\theta_r+\frac{\pi}{Q_r}\right) & (1-\mu)\cos\left(\theta_r+\frac{3\pi}{Q_r}\right) & (1-\mu)\cos\left(\theta_r+\frac{5\pi}{Q_r}\right) & \cdots & (1-\mu)\cos\left(\theta_r+\frac{(2Q_r-1)\pi}{Q_r}\right)\\ \cos\left(\theta_r+\frac{\pi}{Q_r}-\frac{2\pi}{3}\right) & \cos\left(\theta_r+\frac{3\pi}{Q_r}-\frac{2\pi}{3}\right) & \cos\left(\theta_r+\frac{5\pi}{Q_r}-\frac{2\pi}{3}\right) & \cdots & \cos\left(\theta_r+\frac{(2Q_r-1)\pi}{Q_r}-\frac{2\pi}{3}\right)\\ \cos\left(\theta_r+\frac{\pi}{Q_r}+\frac{2\pi}{3}\right) & \cos\left(\theta_r+\frac{3\pi}{Q_r}+\frac{2\pi}{3}\right) & \cos\left(\theta_r+\frac{5\pi}{Q_r}+\frac{2\pi}{3}\right) & \cdots & \cos\left(\theta_r+\frac{(2Q_r-1)\pi}{Q_r}+\frac{2\pi}{3}\right)\\ (\mu)\cos\left(\theta_r+\frac{\pi}{Q_r}\right) & (\mu)\cos\left(\theta_r+\frac{3\pi}{Q_r}\right) & (\mu)\cos\left(\theta_r+\frac{5\pi}{Q_r}\right) & \cdots & (\mu)\cos\left(\theta_r+\frac{(2Q_r-1)\pi}{Q_r}\right)\end{bmatrix}, \tag{22}$$

$$\left[L_{s2,r}\right]=m_{sr}\begin{bmatrix}(1-\mu)\cos\left(\theta_r+\frac{\pi}{Q_r}-\alpha\right) & (1-\mu)\cos\left(\theta_r+\frac{3\pi}{Q_r}-\alpha\right) & (1-\mu)\cos\left(\theta_r+\frac{5\pi}{Q_r}-\alpha\right) & \cdots & (1-\mu)\cos\left(\theta_r+\frac{(2Q_r-1)\pi}{Q_r}-\alpha\right)\\ \cos\left(\theta_r+\frac{\pi}{Q_r}-\frac{2\pi}{3}-\alpha\right) & \cos\left(\theta_r+\frac{3\pi}{Q_r}-\frac{2\pi}{3}-\alpha\right) & \cos\left(\theta_r+\frac{5\pi}{Q_r}-\frac{2\pi}{3}-\alpha\right) & \cdots & \cos\left(\theta_r+\frac{(2Q_r-1)\pi}{Q_r}-\frac{2\pi}{3}-\alpha\right)\\ \cos\left(\theta_r+\frac{\pi}{Q_r}+\frac{2\pi}{3}-\alpha\right) & \cos\left(\theta_r+\frac{3\pi}{Q_r}+\frac{2\pi}{3}-\alpha\right) & \cos\left(\theta_r+\frac{5\pi}{Q_r}+\frac{2\pi}{3}-\alpha\right) & \cdots & \cos\left(\theta_r+\frac{(2Q_r-1)\pi}{Q_r}+\frac{2\pi}{3}-\alpha\right)\\ (\mu)\cos\left(\theta_r+\frac{\pi}{Q_r}-\alpha\right) & (\mu)\cos\left(\theta_r+\frac{3\pi}{Q_r}-\alpha\right) & (\mu)\cos\left(\theta_r+\frac{5\pi}{Q_r}-\alpha\right) & \cdots & (\mu)\cos\left(\theta_r+\frac{(2Q_r-1)\pi}{Q_r}-\alpha\right)\end{bmatrix}, \tag{23}$$

$$\begin{cases}\left[v_{s1}\right]=\left[r_{s1}\right]\left[i_{s1}\right]+\frac{d}{dt}\left(\left[L_{s1,s1}\right]\left[i_{s1}\right]+\left[L_{s1,s2}\right]\left[i_{s2}\right]+\left[L_{s1,r}\right]\left[i_r\right]\right)\\ \left[v_{s2}\right]=\left[r_{s2}\right]\left[i_{s2}\right]+\frac{d}{dt}\left(\left[L_{s2,s1}\right]\left[i_{s1}\right]+\left[L_{s2,s2}\right]\left[i_{s2}\right]+\left[L_{s2,r}\right]\left[i_r\right]\right), \\ \left[v_r\right]=\left[r_r\right]\left[i_r\right]+\frac{d}{dt}\left(\left[L_{r,s1}\right]\left[i_{s1}\right]+\left[L_{r,s2}\right]\left[i_{s2}\right]+\left[L_{r,r}\right]\left[i_r\right]\right)\end{cases} \tag{24}$$

$$\begin{cases} \dfrac{d}{dt}([i_{s1}]) = [L_{s1,s1}]^{-1}\left\{[v_{s1}]-[r_{s1}][i_{s1}]-[L_{s1,s2}]\dfrac{d}{dt}([i_{s2}])-\omega_r\dfrac{d}{d_{\theta r}}([L_{s1,r}])[i_r]-[L_{s1,r}]([i_r])\right\} \\ \dfrac{d}{dt}([i_{s2}]) = [L_{s2,s2}]^{-1}\left\{[v_{s2}]-[r_{s2}][i_{s2}]-[L_{s2,s1}]\dfrac{d}{dt}([i_{s1}])-\omega_r\dfrac{d}{d_{\theta r}}([L_{s2,r}])[i_r]-[L_{s2,r}]([i_r])\right\} \\ \dfrac{d}{dt}([i_r]) = [L_{r,r}]^{-1}\left\{[v_r]-[r_r][i_r]-\omega_r\dfrac{d}{d_{\theta r}}([L_{r,s1}])[i_{s1}]-[L_{r,s1}]\dfrac{d}{dt}([i_{s1}])-\omega_r\dfrac{d}{d_{\theta r}}([L_{r,s2}])[i_{s2}]-[L_{r,s2}]\dfrac{d}{dt}([i_{s2}])\right\} \end{cases} . \quad (25)$$

From the results obtained, it is clear that the presence of two adjacent broken bars has a significant impact on various aspects of machine performance. Fig. 4 and 5 illustrate the evolution of speed and torque as a function of time.

The transition from no-load to loaded operation at time t = 1.5 s is almost instantaneous, with no significant oscillations and a slight overshoot. A slight fluctuation is observed when the first rotor bar breaks (at time t = 3 s). This fluctuation, which intensifies when the second fault occurs (at time t = 4.5 s), oscillates at a frequency of 2 gfs. This speed variation is very small, as it depends mainly on the inertia of the machine-load assembly. The greater the inertia of this assembly, the less significant the speed variation. Analysis of the electromagnetic torque reveals a noticeable change in its shape when rotor faults occur. A slight modulation disturbs the evolution of torque when the first bar breaks. Moreover, this modulation becomes more pronounced with the appearance of the second fault. When analyzing stator current responses before and after bar breakage, stator current modulation increases significantly with the number of broken bars (Fig. 6 and 7). Fig. 8 shows the rotor currents in the first three rotor bars. It can be seen that the current in the first bar cancels out at t = 3 s. Similarly, the second bar current cancels out at t = 4.5 s. Fig. 9 show the distribution of currents through the rotor bars at time t for the three operating modes studied: healthy rotor, one broken bar and two broken bars. We can see that breaking the first bar induces a very slight increase in the current flowing through it. At the moment of the first fault, the current flowing through the broken bar is shared by the adjacent rotor bars. When the second bar is broken, the current in bar 3 increases significantly.

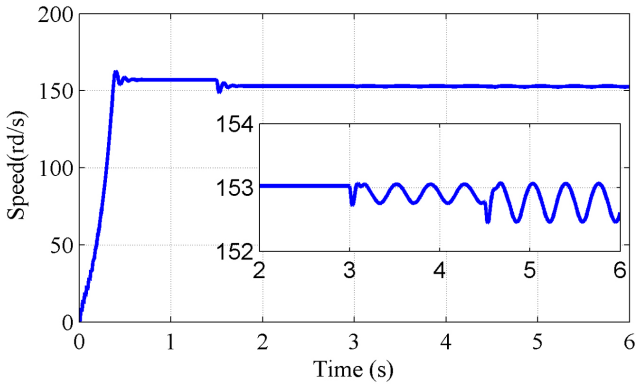

Fig. 4 Machine speed

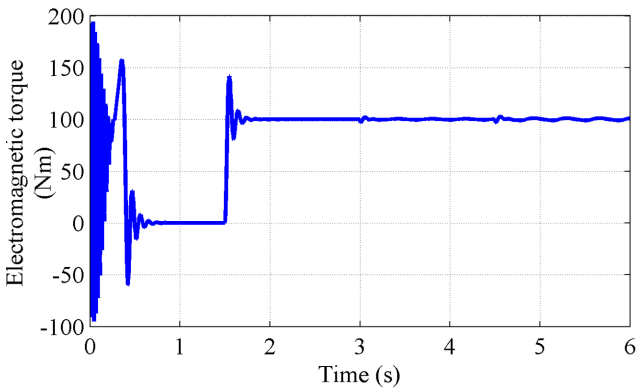

Fig. 5 Machine torque

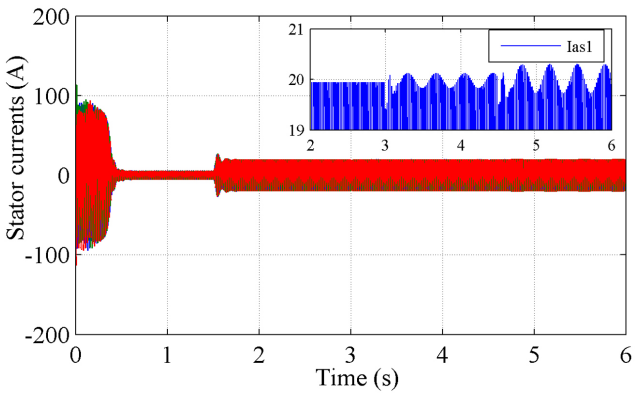

Fig. 6 Currents from the 1st star

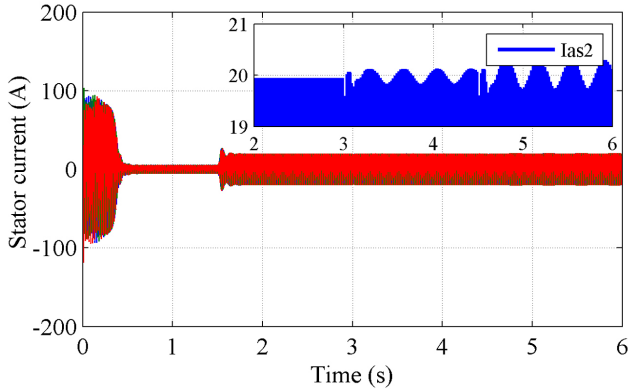

Fig. 7 Currents from the 2nd star

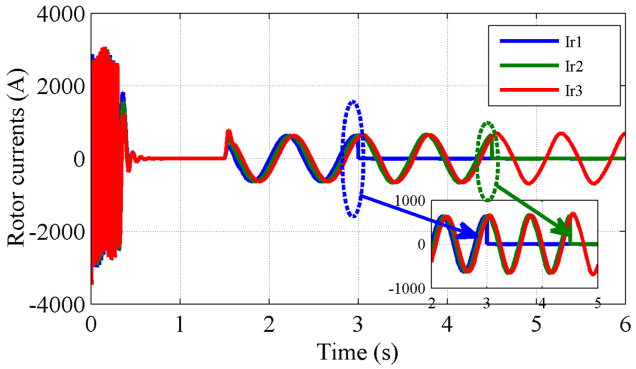

Fig. 8 Rotor-bar currents 1, 2 and 3

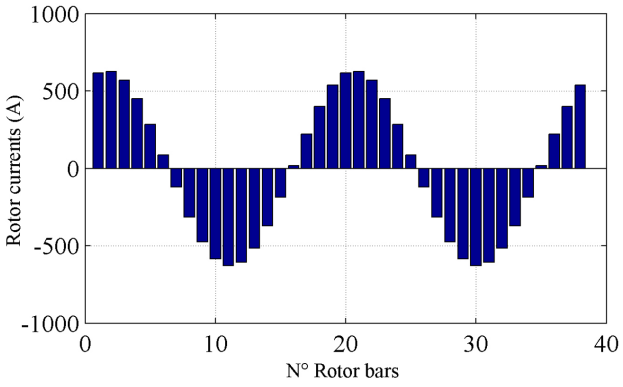

(A)

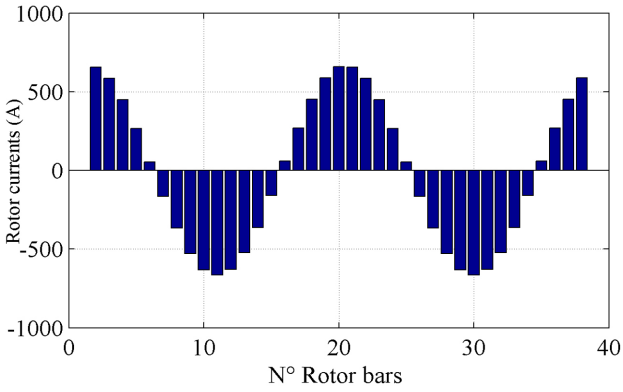

(B)

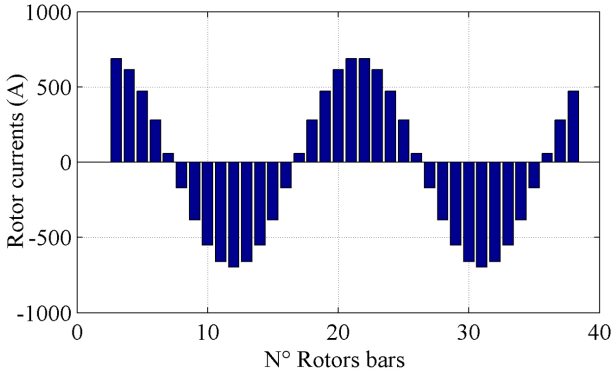

(C)

Fig. 9 Currents repartition in the rotor bars at time *t*:
(A) Sound rotor; (B) First broken bar; (C) Second broken bar

3.2 Analysis of simulation results in the presence of a stator phase opening fault

No major changes to the fundamental structure of the model are required to simulate a phase disconnection, with the exception of increasing the resistance of the phase affected by the disconnection to a very high value, thus simulating an open circuit. This will enable the machine's steady-state behavior to be predicted immediately after the fault.

The simulation results are presented as shown in Figs (10–13). At time $t = 1.5$ s, a load torque of 50 N.m was applied, representing 50% of the nominal torque. The aim of this measure is to prevent damage to the machine and

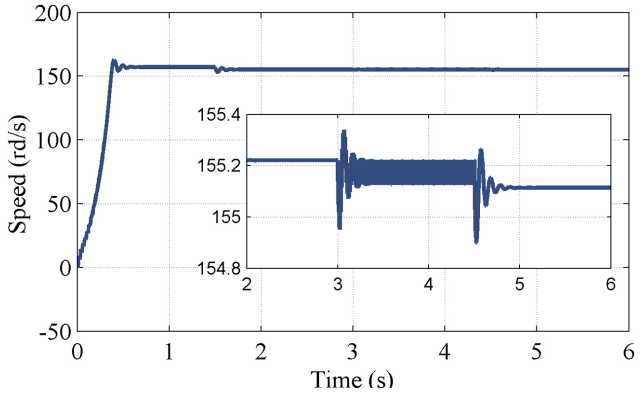

Fig. 10 Speed machine

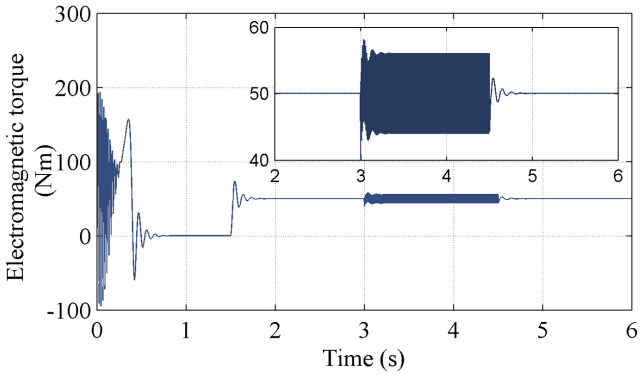

Fig. 11 Torque machine

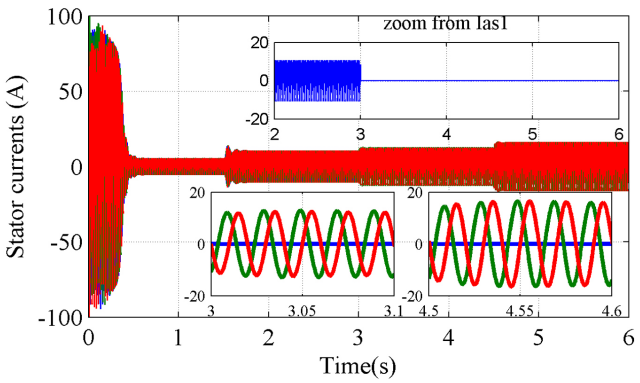

Fig. 12 Currents from the 1st star

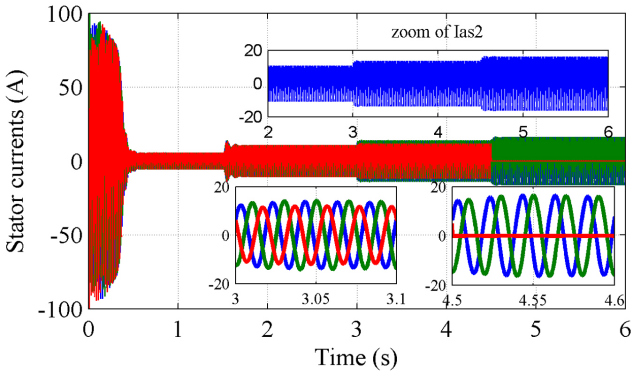

Fig. 13 Currents from the 2nd star

ensure that it operates correctly in real-life conditions. To demonstrate the advantages of using the model in the natural reference frame, the first phase of star 1 opened at t = 3 s. This led to deterioration in the performance of the machine under study and always results in unbalanced stator currents projected onto the electromagnetic torque and mechanical speed. At t = 4.5 s, to remedy the opening of the stator phase, the third phase c_{s2} of star 2 was opened, this being adjacent to the first phase of star 1.

This action generates sinusoidal currents with amplitudes approximately equivalent to those in healthy operation. The rotor currents, electromagnetic torque and rotor speed oscillate for a given period. However, when the third phase of star 2 opens, the curves return to their usual stable configuration for torque and speed, synchronized with the mains frequency. In addition, the currents adopt sinusoidal shapes, similar to their normal behavior.

3.3 Simulation and interpretation of DSIM results in the presence of a short circuit between turns in the stator phase (as)

To examine inter-turn short fault with rates of 5%, 15%, and 25% respectively, simulations were carried out by inducing front-end short-circuits exclusively on the as phase winding, considering a fault resistance (r_{f1} = 0). The simulation was carried out during a no-load start-up, with the electromagnetic torque applied at time (t = 1.5 s). Fig. 14 shows the speed, which is initially quasi-linear at the start of start-up, with a speed-up time of approximately 0.25 s. Fig. 15 illustrates the behaviour of the generator's electromagnetic torque, showing fluctuations around 50 N.m, as the machine is under load. Ripples in the torque show the harmful impact of the short- circuit on the machine's performance. A noticeable increase in the amplitude of the current in the faulty phase is observed, with an equally noticeable increase in the currents in the other phases, although

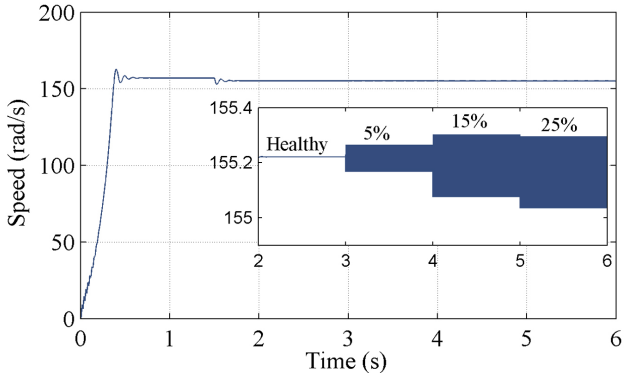

Fig. 14 Speed machine

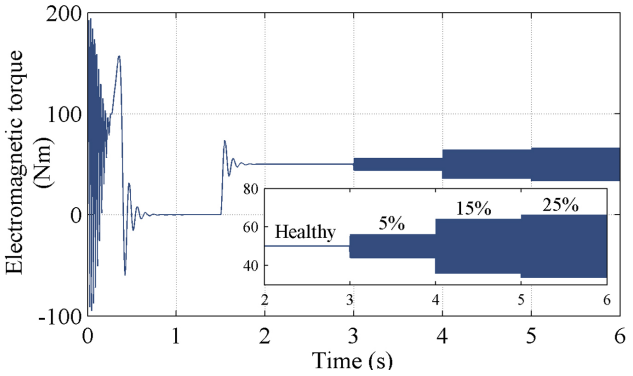

Fig. 15 Torque machine

less significant than in the affected phase (Fig. 16). In addition, the rotor currents increase, as shown in Fig. 17.

3.4 Spectral analysis of all signals obtained under different operating conditions

In this study, the stator current, the torque and the rotating speed signals spectra obtained from three distinct motors running at a consistent speed and load are analyzed. As revealed in the Fig. 18 (A), the amplitude of the modulated frequencies $(1 \pm 2ks)\, f_s$ in the current spectrum increases directly with the severity of the broken rotor bar fault. Concurrently, the amplitude of the frequency $2ks\, f_s$

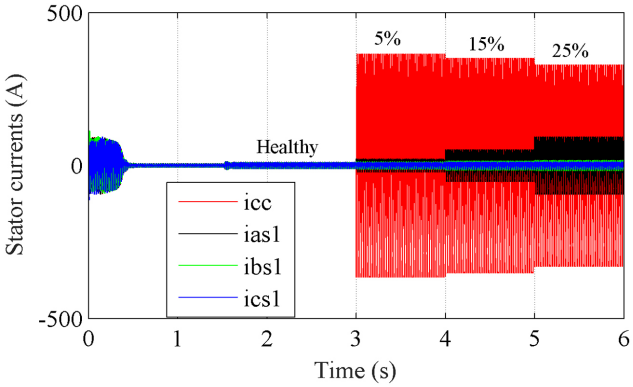

Fig. 16 Currents from the 1st star

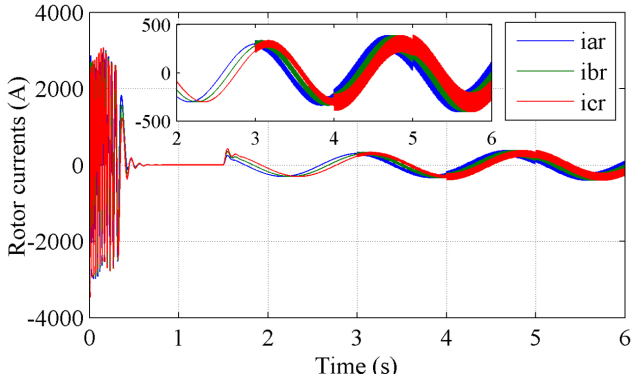

Fig. 17 Rotor-bar currents 1, 2 and 3

phase to the preceding one remained effective to eliminate all components resulting from the OP fault.

4 Conclusion

The research presented here represents a significant contribution to the study of faults occurring in a double-star asynchronous machine. The study focused mainly on electrical faults, including rotor bar breakage, stator phase opening and short circuits. The mathematical equations defining the machine's behavior were formulated in the natural reference frame of reference (ABC), meticulously

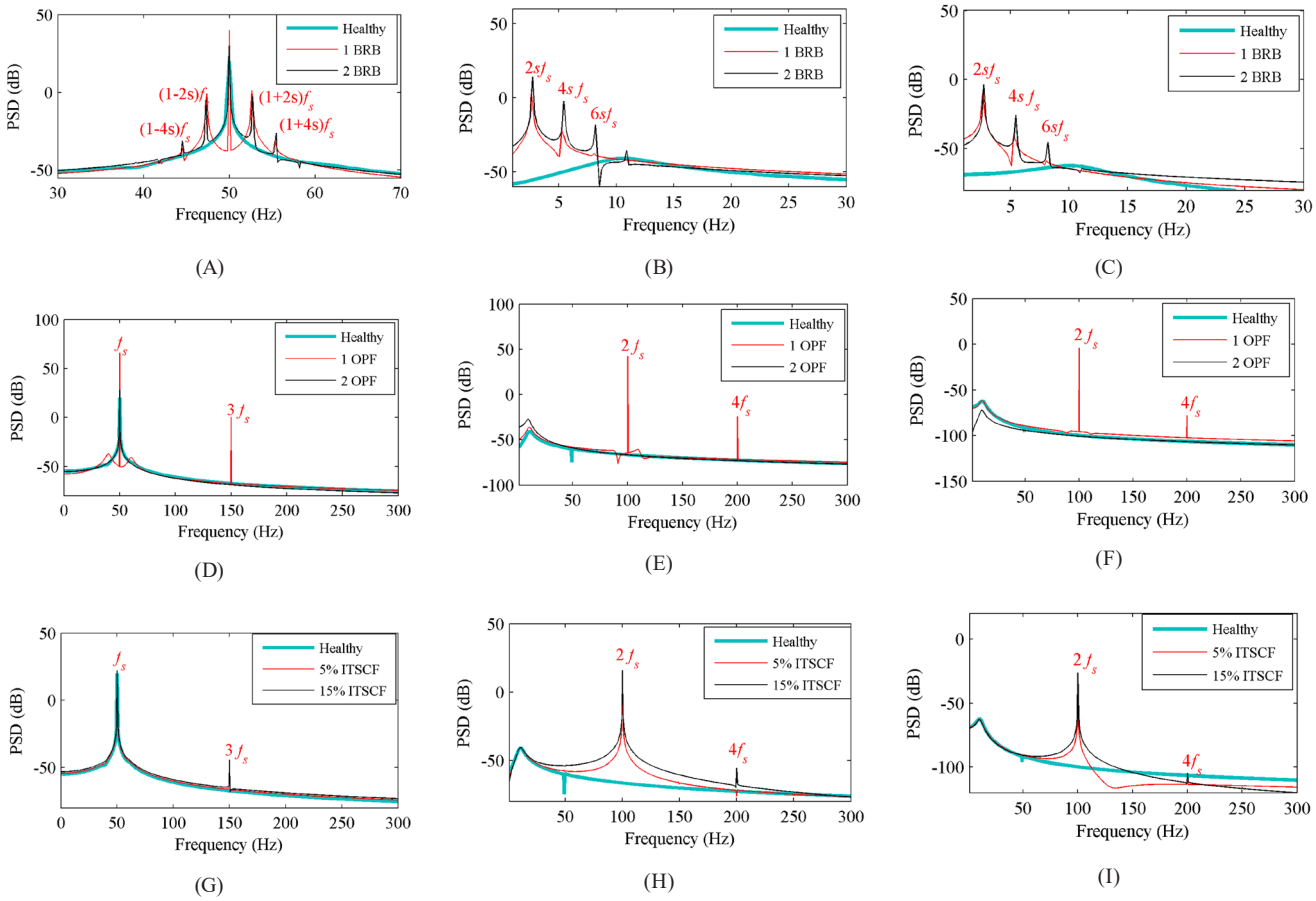

Fig. 18 Fig. 18The spectra of the resulting signals: (A) the stator current under broken rotor bars fault, (B) the rotating speed under broken rotor bars fault, (C) the torque under broken rotor bars fault, (D) the stator current under open phase fault, (E) the rotating speed under open phase fault, (F) the torque under open phase fault, (G) the stator current under interturn short-circuit fault, (H) the rotating speed under interturn short-circuit fault, (I) the torque under interturn short-circuit fault

and its harmonics of both torque and speed spectra increases proportionally to the fault severity, see Fig. 18 (B).

When the opening stator phase fault (OPF) occurs, the different spectra are calculated and showed in Fig. 18 (D-F). The amplitude of the 3rd harmonic in the current spectrum increases compared to the healthy current. A similar trend is noticed in torque and speed spectra, where components at the frequency ($2f_s$) and its harmonic appear. However, simultaneously opening the adjacent

adapted to the purpose of fault diagnosis. Note that in the abc reference frame, each term of the inductance matrix is adjusted as a function of the electrical angle, enabling precise modeling of the system. This model is particularly effective for studying machine behavior in the event of a fault, as it can be easily configured to describe different types of faults without the need for additional calculations. In addition, it enables the machine's performance to be

analyzed both under normal conditions and in the event of a fault, simplifying the evaluation of its operation in different scenarios. Consequently, we generated plots elucidating the machine's characteristics under both fault-free conditions and instances where faults were present, there by accentuating the discernible impact of these faults. Our findings unveiled that: Rotor bar breaks elicit oscillations in the machine's torque and speed, a slight elevation in the amplitude of rotor bar currents, and the emergence of harmonics in the stator currents. It is imperative to emphasize that detecting bar breaks under no-load conditions is intricate. The opening of a stator phase disrupts the machine's normal operation, inducing fluctuations in torque and speed. To address a potential phase loss and ensure continuous machine operation, a proposed solution entails opening a second phase of star 2, adjacent to the first phase (forming a 90° angle), thereby transforming the machine into a dual-phase, double-star configuration. However, detecting short circuits proves to be equally challenging, either through direct measurement of stator current or by activating overload protection on the remaining phases. To mitigate this issue, one avenue explored involves spectral analysis of the stator current, which assumes a pivotal role as detailed in this study. It is noteworthy that the machine's mathematical model developed herein has demonstrated its efficacy when compared to similar research endeavors.

References

[1] Rahman, U. M., Munim, W. N., Che, H. S., Tousizadeh, M., Muhammad, K. S. "Fault tolerance of asymmetrical six-phase induction machine during single open circuit fault to three open circuit faults using GUI", International Journal of Power Electronics and Drive Systems, 11(2), pp. 611–617, 2020. https://doi.org/10.11591/ijpeds.v11.i2.pp611-617

[2] Azib, A., Ziane, D. "A highly effective modified direct torque control for five phase induction motor without ac phase current sensors", Periodica Polytechnica Electrical Engineering and Computer Science, 67(1), pp. 1–9, 2023. https://doi.org/10.3311/PPee.20384

[3] Chekkal, S., Lahaçani, N. A., Aouzellag, D., Ghedamsi, K. "Fuzzy logic control strategy of wind generator based on the dual-stator induction generator", International Journal of Electrical Power and Energy Systems, 59, pp. 166–175, 2014. https://doi.org/10.1016/j.ijepes.2014.02.005

[4] Hamitouche, K., Chekkal, S., Amimeur, H., Aouzellag, D. "A new control strategy of dual stator induction generator with power regulation", Journal Européen des Systèmes Automatisés, 53(4), pp. 469–478, 2020. https://doi.org./10.18280/jesa.530404

[5] Moati, Y., Kouzi, K. "Investigating the performances of direct torque and flux control for dual stator induction motor with direct and indirect matrix converter", Periodica Polytechnica Electrical Engineering and Computer Science, 64(1), pp. 97–105, 2020. https://doi.org/10.3311/PPee.14977

[6] Maanani, Y., Menacer, A. "Modeling and diagnosis of the inter-turn short circuit fault for the sensorless input-output linearization control of the PMSM", Periodica Polytechnica Electrical Engineering and Computer Science, 63(3), pp. 159–168, 2019. https://doi.org/10.3311/PPee.13658

[7] Bonnett, A. H., Soukup, G. C. "Cause and analysis of stator and rotor failures in three-phase squirrel-cage induction motors", IEEE Transactions on Industry Applications, 28(4), pp. 921–937, 1992. https://doi.org/10.1109/28.148460

[8] Ojaghi, M., Sabouri, M., Faiz, J. "Diagnosis methods for stator winding faults in three-phase squirrel-cage induction motors", International Transactions on Electrical Energy Systems, 24(6), pp. 891–912, 2014. https://doi.org/10.1002/etep.1750

[9] Schoen, R. R., Lin, B. K., Habetler, T. G., Schlag, J. H., Farag, S. "An unsupervised, on-line system for induction motor fault detection using stator current monitoring", IEEE Transactions on Industry Applications, 31(6), pp. 1280–1286, 1995. https://doi.org/10.1109/28.475698

[10] Tavner, P. J. "Review of condition monitoring of rotating electrical machines", IET Electric Power Applications, 2(4), pp. 215–247, 2008. https://doi.org/10.1049/iet-epa:20070280

[11] Didier, G., Ternisien, E., Caspary, O., Razik, H. "A new approach to detect broken rotor bars in induction machines by current spectrum analysis", Mechanical Systems and Signal Processing, 21(2), pp. 1127–1142, 2007. https://doi.org/10.1016/j.ymssp.2006.03.002

[12] Ridha, K., Arezki, M., Hakima, C. "Broken rotor bars fault detection in induction motors using FFT: simulation and experimentally study", Algerian Journal of Engineering and Technology, 1, pp. 19–24, 2019. https://doi.org/10.5281/zenodo.3595143

[13] Arabaci, H., Mohamed, M. A. "A knowledge-based diagnosis algorithm for broken rotor bar fault classification using FFT, principal component analysis and support vector machines", International Journal of Intelligent Engineering Informatics, 8(1), pp. 19–37, 2020. https://doi.org/10.1504/IJIEI.2020.105431

[14] Abd-el-Malek, M., Abdelsalam, A. K., Hassan, O. E. "Induction motor broken rotor bar fault location detection through envelope analysis of start-up current using Hilbert transform", Mechanical Systems and Signal Processing, 93, pp. 332–350, 2017. https://doi.org/10.1016/j.ymssp.2017.02.014

[15] Gangsar, P., Tiwari, R. "Signal based condition monitoring techniques for fault detection and diagnosis of induction motors: A state-of-the-art review", Mechanical Systems and Signal Processing, 144, 106908, 2020. https://doi.org/10.1016/j.ymssp.2020.106908

[16] Dehina, W., Boumehraz, M. "Experimental investigation in induction motors using signal processing techniques for early detection of inter-turn short circuit faults", International Journal of Modelling and Simulation, 42(5), pp. 855–867, 2022. https://doi.org/10.1080/02286203.2021.2001635

[17] dos Santos, T., Ferreira, F. J. T. E., Pires, J. M., Damásio, C. "Stator winding short-circuit fault diagnosis in induction motors using random forest", 2017 IEEE International Electric Machines and Drives Conference (IEMDC), Miami, FL, USA, pp. 1–8, 2017. https://doi.org/10.1109/IEMDC.2017.8002350

[18] Dongare, U., Umre, B., Ballal, M. "Stator inter-turn short-circuit fault diagnosis in induction motors applying VI loci-based technique", Energy Reports, 9, pp. 1483–1493, 2023. https://doi.org/10.1016/j.egyr.2023.06.043

[19] Alawady, A. A., Yousof, M. F. M., Azis, N., Talib, M. A. "Frequency response analysis technique for induction motor short circuit faults detection", International Journal of Power Electronics and Drive Systems, 11(3), pp. 1653–1659, 2020. https://doi.org/10.11591/ijpeds.v11.i3.pp1653-1659

[20] Radhi, A. T., Zayer, W. H. "Faults diagnosis in stator windings of high speed solid rotor induction motors using fuzzy neural network", International Journal of Power Electronics and Drive Systems, 12(1), pp. 597–611, 2021. https://doi.org/10.11591/ijpeds.v12.i1.pp597-611

[21] Guettab, A., Boudjema, Z., Bounadja, E., R. Taleb, "Improved control scheme of a dual star induction generator integrated in a wind turbine system in normal and open-phase fault mode", Energy Reports, 8, pp. 6866–6875, 2022. https://doi.org/10.1016/j.egyr.2022.05.048

[22] Khadar, S., Kouzou, A., Rezzaoui, M. M., Hafaifa, A. "Sensorless control technique of open-end winding five phase induction motor under partial stator winding short-circuit", Periodica Polytechnica Electrical Engineering and Computer Science, 64(1), pp. 2–19, 2020. https://doi.org/10.3311/PPee.14306

[23] Pyrhonen, J., Jokinen, T., Hrabovcova, V. "Design of rotating electrical machines", John Wiley and Sons, 2013. https://doi.org/10.1002/9781118701591

[24] MathWorks, Inc. "MATLAB and SIMULINK, (R2015b)", [computer program] Available at: https://www.mathworks.com/products/matlab.html [Accessed: 30 June 2024]